Case Studies in Thermal Engineering 65 (2025) 105665

Contents lists available at ScienceDirect

Case Studies in Thermal Engineering

journal homepage: www.elsevier.com/locate/csite

Experimental and numerical assessment of water-based photovoltaic/thermal collectors with varied tubular absorber cross-sections

Shirin Rostami [a], Adnan Ibrahim [a,*], Amir Aziat Ishak [b], Ahmad Fazlizan [a], Ahmad Fudholi [a], Kamaruzzaman Sopian [c], Alireza Dehghani-Sanij [d], Amin Shahsavar [e], Khaled M. Al-Aribe [f]

[a] *Solar Energy Research Institute, Universiti Kebangsaan Malaysia (UKM), Bangi, 43600, Selangor, Malaysia*
[b] *School of Engineering, Faculty of Innovation & Technology, Taylor's University Lakeside Campus, Subang Jaya, Selangor, Malaysia*
[c] *Department of Mechanical Engineering, Universiti Teknologi Petronas (UTP), Seri Iskandar, 32610, Perak, Malaysia*
[d] *Waterloo Institute for Sustainable Energy (WISE), University of Waterloo, Waterloo, ON, N2L 3G1, Canada*
[e] *Department of Mechanical Engineering, Kermanshah University of Technology, Kermanshah, Iran*
[f] *Department of Mechanical and Industrial Engineering, Abu Dhabi University, Abu Dhabi, 59911, United Arab Emirates*

ARTICLE INFO

Keywords:
PV/T collector
Heat transfer
Hydraulic diameter
3D numerical model

ABSTRACT

This study aims to develop 3D numerical models utilizing COMSOL software to analyze the heat transfer (HT) behaviour of water-based photovoltaic/thermal (WPV/T) collectors with circular, and elliptical tubular cross-sections with different dimensions to find an optimized and efficient PV/T design. Indoor experimental tests were conducted to validate the numerical results. The performance of PV/T was evaluated in terms of governing parameters, including the mass flow rate ($\dot{m}$), solar irradiance (I), heat gain, maximum power (P_{max}), Reynolds number (Re), thermal (η_{th}) and electrical (η_{el}) efficiency, the temperature difference between the outlet and inlet water (T_o-T_i), the average cell temperature, and total efficiency (η_{total}). It was determined that $\dot{m} = 0.04$ kg/s was the optimal water flow rate for the best performance. The results indicate that the PV/T collector with the elliptical cross-section tube with the least hydraulic diameter achieved the maximum total efficiency, both numerically and experimentally, at 76.9 % and 72.94 %, respectively, under turbulent flow conditions with $Re = 5502.92$ and $I = 1000$ W/m^2. η_{total} of the elliptical PV/T collectors is approximately 10 % and 6 % higher than that of circular design, respectively at the optimum flow rate, and $I = 1000$ W/m^2. It is also found that tubes with lower hydraulic diameter values, while maintaining the same tube cross-section perimeter, exhibit higher HT characteristics compared to those with greater hydraulic diameters. The findings from this innovative and comprehensive study indicate an opportunity to enhance the HT properties of the PV/T system by optimizing the cross-sectional design and hydraulic diameter of the absorber tube, ultimately increasing total efficiency. Additionally, the optimized design opens avenues for future research and can be further developed for both industrial and domestic applications.

* Corresponding author.
E-mail address: iadnan@ukm.edu.my (A. Ibrahim).

https://doi.org/10.1016/j.csite.2024.105665
Received 22 August 2024; Received in revised form 21 November 2024; Accepted 18 December 2024
Available online 18 December 2024

1. Introduction

The concept of PV/T systems was first presented in the 1970s, and since then, it has been the subject of extensive research for nearly five decades [1–6]. Conventional PV/T systems comprise a PV module coupled with a solar thermal collector affixed to the rear of the PV panel. This collector extracts heat from the panel through a highly absorptive surface and transfers it to a working fluid that circulates naturally or with an external force inside the flow channel [7–10]. The acquired heat supplies various applications, such as providing hot water, meeting industrial energy demand, and energy-intensive processes such as space heating, cooling, drying, and those operating at temperatures below 100 °C [11–13]. A PV/T system generates electrical and thermal energy simultaneously as a combined unit. Since PV panels' efficiency drops at a rate of 0.4–0.65 percent per degree rise in temperature, the cooling effects of working fluids lead to heat dissipation of the PV panel, enabling a PV/T unit to produce higher electrical efficiency than a distinct PV panel unit [14–18].

Designing efficient and reliable PV/T systems relies heavily on the HT rate between the thermal collector and the PV module, and it largely depends on various parameters, encompassing the thermal collector's geometry, its integration with the PV module, the thermal characteristics of coolant fluids, and the system configuration [19–25]. When it comes to cooling PV/T systems, water is by far the most common working fluid owing to its low cost, abundance, and superior thermal properties compared to air [26–28]. Dissipating heat from PV panels using air as a coolant is straightforward and economical. However, its effectiveness diminishes in low latitudes during multiple months of the year when the ambient temperature (T_{amb}) surpasses 20 °C [29–32]. Recent reviews have illustrated that a typical WPV/T system can attain electrical and thermal efficiencies of 10–12 % and 33–72 %, respectively, greater than air-based PV/T systems [13,33–37]. Water as a cooling medium in PV/T systems has been extensively researched and developed from various perspectives globally. The performance of a WPV/T collector mainly depends on parameters such as $\dot{m}$, the thermal collector's geometry, inlet (T_i) and outlet (T_o) water temperatures, solar radiation, and ambient conditions. Many researchers have studied these influential parameters to design and develop the most efficient systems [16,28,38–41]. Nahar et al. [42] conducted outdoor tests and numerical simulation using COMSOL software to study an innovative parallel plate PV/T collector design. The study concluded that η_{el} reduced from 12.6 to 11.3 % in numerical simulations and from 12 to 10 % in experimental tests within $500 < I < 1000$ W/m^2. The maximum η_{total} of the systems was found to be 80 % in experimental investigations and 84.4 % in numerical simulations, both achieved under $I = 1000$ W/m^2, with T_i and T_{amb} at 34 °C. Yazdanifard et al. [43] simulated the WPV/T systems for laminar and turbulent flows using MATLAB software. The findings revealed that as the intensity of I rose from 300 to 1000 W/m^2, η_{total} increased for both laminar and turbulent flows. Moreover, in most cases, turbulent flow (higher $\dot{m}$) resulted in greater η_{total} than laminar flow. Hajji et al. [32] developed an energy-balanced mathematical model for a WPV/T collector. The findings demonstrated that the PV module surface temperature dropped from 84 °C to 34 °C as $\dot{m}$ rose from 0.01 to 0.1 kg/s, while η_{th} and η_{el} improved. Although η_{el} declined as solar radiation increased, η_{th} showed an upward trend.

Many investigations have concluded that raising the $\dot{m}$ may enhance a WPV/T system's overall performance. While higher $\dot{m}$ may lead to higher efficiency, Jarimi et al. [44] highlighted the importance of determining a PV/T's optimal $\dot{m}$. They emphasized that it is essential for a system to operate with the optimal flow rate of coolants to achieve the best performance. Abdullah et al. [45] conducted indoor experiments and simulations using MATLAB software to assess a new dual oscillating absorber in a WPV/T system and compared the results to those of a standard PV panel with no cooling system. The system's performance was evaluated within $500 < I < 1000$ W/m^2 and at various $\dot{m}$ ranging from 2 to 6 L per minute (LPM). 11.5 % was the maximum η_{el} at $\dot{m} = 6$ LPM and $I = 500$

Table 1
Literature reviews on serpentine designs with different cross-sections.

Authors	Year of study	Type of study	Location	Tube cross-section	Remarks of non-circular cross-sections study
Xu et al. [48]	2020	Experimental	China	Circular	
Korres and Tzivanidis [49]	2018	Theoretical	Greece	Circular	
Shah et al. [50]	2018	Experimental and 2D simulation	India	Circular	
Mohammadi Sardouie et al. [51]	2018	Experimental and 3D simulation	Iran	Circular and square	They discovered that, due to the wider contact surface, the square cross-sectional tube exhibited a higher heat transfer rate than the round tube.
Al-Waeli et al. [52]	2017	Experimental	Malaysia	Circular	
Jarimi et al. [44]	2016	Theoretical and experimental	Malaysia	Circular	
Rosli et al. [53]	2014	Theoretical	Malaysia	Circular, rectangular, and square	They concluded that the heat transfer capability of the rectangular cross-section was superior when compared to both circular and square cross-sections.
Kumar [54]	2014	Theoretical	India	Semi-circular	The author found that semi-circular cross-sectional tubes absorb more heat than their circular counterparts.
Razi et al. [55]	2011	Experimental	Malaysia	Circular and flattened	They discovered that, at the same flow rates, flattened tube collectors had a much higher heat transfer coefficient than circular tubes.
Ibrahim et al. [56]	2009	Theoretical and 3D simulation	Malaysia	Circular	

W/m^2. At $I = 1000$ W/m^2 and $\dot{m} = 5$ LPM, the highest η_{th} and η_{total} were determined to be 58.64 % and 66.87 %, respectively. It was found that both η_{th} and η_{total} improved as $\dot{m}$ increased but declined after the optimal value was attained. Abdul-Ganiyu et al. [1] mentioned that although the PV/T efficiency is directly governed by $\dot{m}$, various studies have suggested an optimum flow rate ranging from 0.001 to 0.008 kg/s. Higher values (0.025–0.04 kg/s) have been recommended for PV/T systems integrated into buildings.

Experimental and numerical findings have suggested that increasing the contact area between the PV module and the absorber tube substantially enhances HT and the PV/T total efficiency [46,47]. Despite this, the development of PV/T designs featuring diverse and efficient cross-sections has been the subject of a limited number of studies, as illustrated in Table 1, HT enhancement in conventional cooling applications, such as PV/T systems, is significantly dependent on the cross-section of absorber tubes employed in thermal collectors.

The PV/T units using circular absorber tube configurations for cooling the PV panels have been explored in many studies. However, innovative and comprehensive research on collectors with effective cross-sections and hydraulic diameters (D_h) to enhance heat transfer in PV/T systems has been lacking. There is also a gap in comprehensive 3D simulations for PV/T systems that can accurately estimate effective tube geometry. This paper addresses these research gaps and assesses an optimized system by conducting 3D numerical simulations using COMSOL software. These simulations comprehensively analyzed and compared the HT behaviour of water-based serpentine PV/T collectors with circular, and two types of elliptical tube cross-sections with different dimensions. The simulation results were validated through indoor experimental findings. The PV/T units' performance was assessed in terms of $\dot{m}$, I, heat gain, P_{max}, Re, η_{th}, η_{el}, T_o-T_i, and η_{total} *and* the average cell temperature. The optimized absorber tube configuration could pave the way for additional studies in the field of PV/T technology and has the potential to be applied in both industrial and household settings.

2. Methodology

2.1. PV/T collector designs

The system designs comprise 50 W monocrystalline PV modules and copper serpentine thermal collectors with elliptical, and circular tube cross-sections. The longer tube length of a serpentine tube allows water to dwell in the collector for longer, resulting in greater fluid temperature differences throughout the system. The serpentine designs optimize thermal stratification in the water tanks, reduce manufacturing expenses, and remain efficient even at low flow rates. Fig. 1 shows a 3D view of these solar thermal collectors. To prevent gaps and maximize heat transmission, copper tubes were affixed to the back of the PV modules using thermal adhesive. Thermal insulating material was applied to the rear of the PV/T collector to mitigate heat loss. The PV modules comprise the following layers: glass, ethylene vinyl acetate (EVA), PV cell, EVA, and Tedlar [57]. Fig. 2 displays the proposed PV/T collectors' cross-sectional view. The design parameters, materials, and thermal characteristics of the PV/Ts are presented in Tables 2 and 3.

2.2. Experimental setups and tests

The indoor experimental setups were installed at the Indoor Solar Simulator Laboratory, National University of Malaysia, to evaluate and compare the thermal and electrical parameters of serpentine WPV/T collectors with circular, and elliptical cross-sections, plus a conventional PV module. Fig. 3 depicts a schematic diagram of the actual setup. The experiments were conducted using a solar simulator comprising 35 (500 W) halogen bulbs. A voltage regulator adjusted the intensity of solar irradiance, providing irradiation levels of 400, 600, 800, and 1000 W/m^2. A solar power meter was employed to measure the irradiance intensity during data collection. Cooling of the PV modules was achieved using a closed-loop water system. A pump forces inlet water from the water tank through a

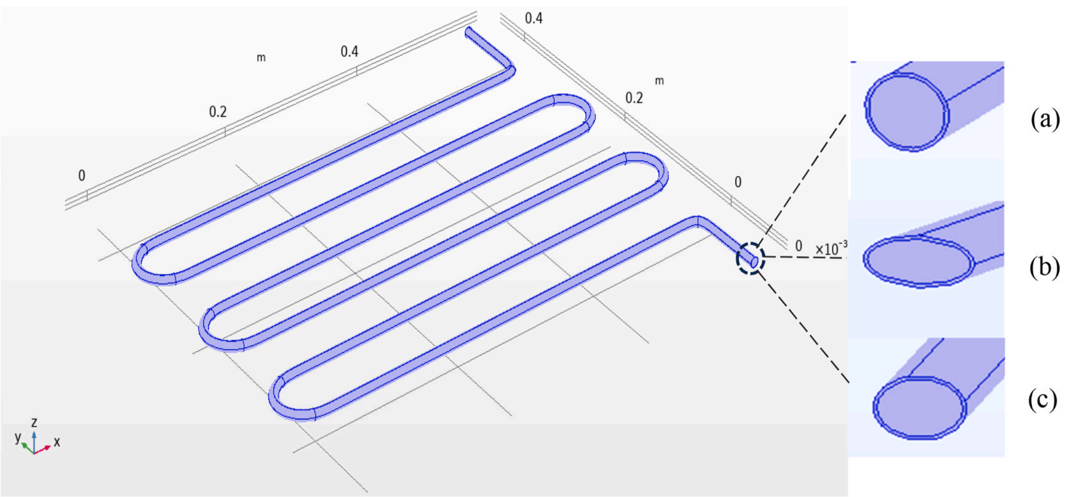

Fig. 1. A 3D view of serpentine collectors with (a) circular, (b) elliptical (type A), and (c) elliptical (type B) cross-sections.

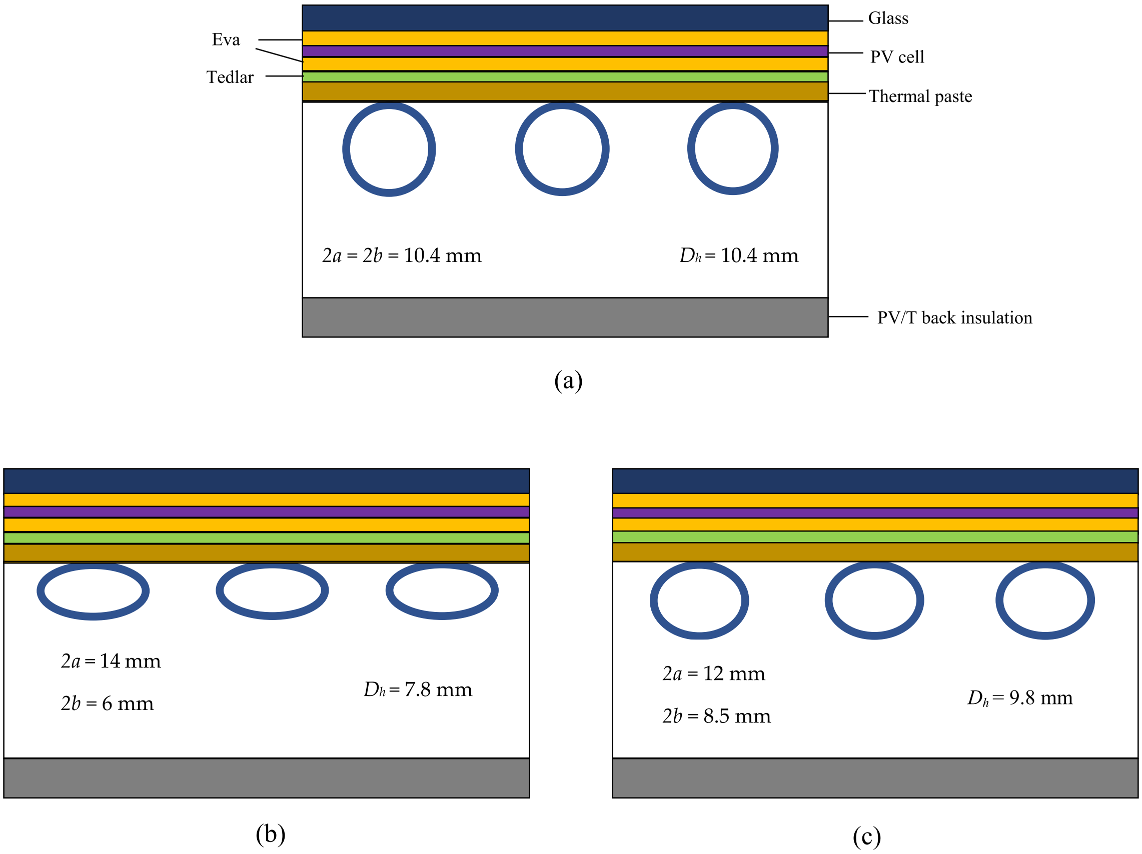

Fig. 2. A cross-sectional view of solar thermal collectors with (a) circular, (b) elliptical (type A), and (c) elliptical (type B) tubes.

Table 2
Design parameters of PV/T components.

PV	Specification
Solar module model	SFM-50
Solar module type	Monocrystalline
Dimension	650 mm × 520 mm × 30 mm
Short-circuit current (I_{sc})	2.53 A
Open-circuit voltage (V_{oc})	21.2 V
Maximum power (P_{max})	50 W
Maximum power voltage (V_{mp})	18 V
Maximum power current (I_{mp})	2.77 A
Serpentine thermal collector	
No. of pipes	6
Length of pipes	56 cm
Space between pipes	60 mm

Table 3
Thermal properties of PV/T components.

Components	Thickness (mm)	Thermal conductivity (W/m.K)	Heat capacity (J/kg.K)	Density (kg/m^3)
Glass	3	2	500	2440
Eva	0.5	0.35	2090	960
PV cell	0.4	148	677	2330
Tedlar	0.1	0.2	1250	1200
Thermal adhesive	2	1.79	500	2400
Copper tubes	1	410	385	8940
Composite insulation	35	0.03	840	16
Water	–	0.60	4181	999

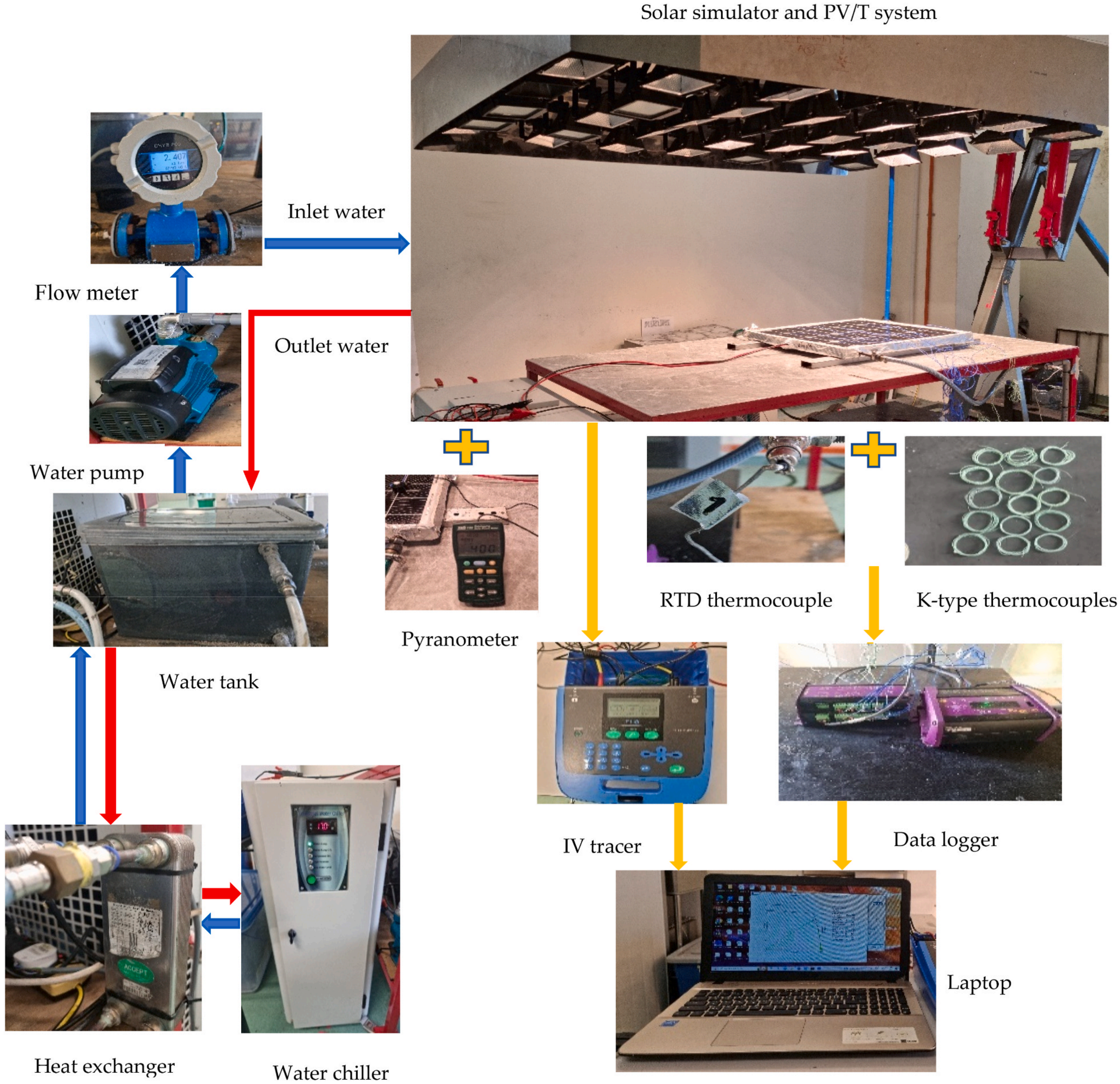

Fig. 3. Actual setup of the proposed PV/T collectors at the Indoor Solar Simulator Laboratory, National University of Malaysia.

Table 4
Experimental equipment list.

Equipment	Model
Water pump	LEO 1HP centrifugal pump
Water chiller	SCP SPH20N-19-4566
Heat exchanger	Brazed plate EATB15
Thermocouples	K-type, RTD PT-100
Flowmeter	DHYB-800
Solar simulator	6CH DMX DIMMER PACK
Pyranometer	Solar power meter TES-132
Data logger	DATA TAKER DT80
IV tracer	I-V CHECKER EKO MP-11

flow meter into the collectors, and precise control of the flow rate was regulated using control valves. The range of inlet water mass flow rates included 0.6, 1.2, 1.8, 2.4, and 3 LPM, corresponding to flow rates of 0.01, 0.02, 0.0.3, 0.04, and 0.05 kg/s. The water absorbed heat from the PV panel and the hot water was circulated through a heat exchanger and then returned to the water tank. Cold water, at a temperature of 17 °C (T_i), was supplied to the heat exchanger by a water chiller. K-type thermocouples were distributed at various points on the PV module's surface to measure the average panel temperature. Inlet and outlet water temperatures were accurately measured using RTD thermocouples. Temperature data from multiple thermocouples were recorded by a data logger at 30-s intervals. The electrical outputs of all systems, namely short-circuit current (I_{sc}), open-circuit voltage (V_{oc}), maximum current (I_{mp}), maximum voltage (V_{mp}), and maximum power (P_{max}) was collected using an IV tracer. A 1-h interval was optimal to establish thermal equilibrium for all systems. The ambient temperature during the experiments was 27 °C. Table 4 provides a summary of the equipment used for the experimental tests.

2.2.1. Governing equations

The η_{th} of a PV/T collector is calculated by Refs. [39,58–60]:

$$\eta_{th} = Q_u / IA_c \tag{1}$$

where Q_u, A_c, and I represent the heat gain, the PV/T collector area, and solar irradiance, respectively.

The useful energy gain is a function of the mass flow rate ($\dot{m}$), fluid specific heat capacity (C_{pf}), and the inlet (T_i) and outlet (T_o) water temperatures, respectively, which are given by:

$$Q_u = \dot{m} C_{pf} (T_o - T_i) \tag{2}$$

The Reynolds number (Re) is defined by Refs. [55,61]:

$$Re = \frac{D_h \dot{m}}{A_{tc} \mu_{df}} = \frac{D_h V_f \rho_f}{\mu_{df}} \tag{3}$$

where D_h, A_{tc}, V_f, ρ_f, and μ_{df} represent the tube hydraulic diameter, tube cross-section area, fluid velocity, fluid density, and fluid dynamic viscosity, respectively. Laminar flow is characterized by $Re < 2300$, transition flow by $2300 < Re < 4000$, and turbulent flow by $Re > 4000$.

The hydraulic diameter (D_h) is a function of the tube cross-sectional area (A_{tc}) and tube cross-sectional perimeter (P_c), which is given by Refs. [52,53]:

$$D_h = 4A_{tc} / P_c \tag{4}$$

For elliptical and oval cross-sections, Eq. (4) can be simplified as follows:

$$D_h = \frac{4ab(64 - 16E^2)}{(a+b)(64 - 3E^4)} \tag{5}$$

where

$$E = \frac{a-b}{a+b} \tag{6}$$

Here, $2a$ and $2b$ represent the major and minor axes of the ellipse and oval, respectively. For a circle, D_h is equivalent to the circle's diameter.

The electrical efficiency can be expressed by equations (7) and (9) [39,60]:

$$\eta_{el} = P_{max} / IA_c \tag{7}$$

which

$$P_{max} = V_{mp} \times I_{mp} \tag{8}$$

$$\eta_{\mathrm{el}} = \eta_{\mathrm{ref}} \left[1 - \beta_{cell} \left(T_{\mathrm{Ave}} - T_{\mathrm{ref}}\right)\right] \tag{9}$$

where η_{ref} is the reference efficiency at the standard conditions ($I = 1000$ W/m^2 and $T_{\mathrm{ref}} = 25$ °C). T_{Ave} is the average cell temperature. β_{cell} is the temperature coefficient of cell and is dependent on materials of PV module. The β_{cell} value for the silicon cell is 0.0045/K.

The total efficiency is calculated by:

$$\eta_{total} = \eta_{el} + \eta_{th} \tag{10}$$

2.3. Numerical simulation

The governing equations are solved using a numerical technique to simulate the systems, known as the finite element method (FEM) in COMSOL software. The following assumptions were considered while creating 3D heat transfer models:

- The heat transfer is considered steady-state $\left(\partial T/\partial t = 0\right)$, and the terms with time derivatives disappear.
- The fluid flowing through the thermal collector is assumed to be incompressible and Newtonian.
- The PV/T collector's thermo-physical characteristics are maintained at a constant value under temperature variation.

The simulation models include solid and fluid domains. The solid domain comprises the PV module layers, insulations, thermal adhesive, and the collector's tube. The fluid domain contains water circulating inside the tube. Table 5 presents all simulation parameters.

2.3.1. Simulation in the solid domain

Heat conduction occurs at the molecular level, and according to Fourier's law of heat conduction, the rate of HT between two solids is directly proportional to the temperature difference between them. This rate of HT per unit area, known as the conductive heat flux (q), is determined as [19,23,40,59]:

$$q = -k\nabla T \tag{11}$$

where ∇T and k denote the temperature gradient and the thermal conductivity, respectively. The negative sign indicates that heat is transferred in the direction of lower temperatures.

Heat transfer in solid domains is solely governed by conduction and is described by:

$$\rho_s c_{ps} u_s.\nabla T + \nabla.q = Q_s + Q_{ted} \tag{12}$$

Here, ρ_s, c_{ps}, u_s, Q_s, and Q_{ted} represent the solid density, the specific heat capacity of the solid phase, the velocity vector of translational motion, additional heat sources, and thermo-elastic damping, respectively.

2.3.2. Simulation in the fluid domain for laminar and turbulent flows

The Navier-Stokes equations, which govern fluid flow and consist of the continuity equation, the momentum equation, and the energy equation, are as follows [22,40,42,59]:

$$\rho_f \nabla.u_f^2 = 0 \tag{13}$$

$$\rho_f\left(u_f^2.\nabla\right)u_f^2 = \nabla.\left[P^2\mathbf{I} + \mu_{df}\left(\nabla u_f^2 + \left(\nabla u_f^2\right)^T\right)\right] + \boldsymbol{F} \tag{14}$$

$$\rho_f c_{pf} u_f.\nabla T^2 + \nabla.q = Q_f + Q_P + Q_{\vartheta d} \tag{15}$$

Here, $P, u_f, \boldsymbol{F}, \mathbf{I}, Q_f, Q_P, \mu_{df},$ and $Q_{\vartheta d}$ represent the pressure, the fluid velocity vector, the volume force, the moment of inertia, heat sources other than viscous dissipation, the work done by pressure changes, the fluid dynamic viscosity, and heat sources via viscous dissipation, respectively.

COMSOL general equations for turbulent flow are based on the Reynolds-Averaged Navier-Stokes equations (RANS), which are modifications of the equations of Navier-Stokes where, instead of the fluid dynamic viscosity term, the fluid effective viscosity $\left(\mu_{eff}\right)$, that is, the sum of fluid dynamic viscosity, and fluid turbulent viscosity (μ_T), is used. Turbulent viscosity of a fluid can be estimated by turbulence models, such as $k-\omega$, $k-\varepsilon$, shear stress transport, etc. The fluid turbulent heat transfer in the present analysis was simulated using the $k-\omega$ model. This model proves to be better for flow geometries, including serpentine pipes that have strong curvature and those with separated boundary layer regions. It is further accurate for near-wall regions, and low Reynolds number turbulent flows. The $k-\omega$ model solves transport equations for the turbulent kinetic energy (K) and the specific dissipation rate (ω) as below:

Table 5
3D simulation parameters.

Parameters	Description
Mass flow rate	0.01, 0.02, 0.03, 0.04 and 0.05 kg/s
Solar irradiance (heat flux)	400, 600, 800, and 1000 W/m^2
Water inlet temperature (T_i)	290 K
Convection to ambient	Heat transfer from outer surface to ambient at $T_{amb} = 300$ K
Heat transfer coefficient	7.1 W/m^2.K

$$\frac{\partial K}{\partial t} + u_f \cdot \nabla K = \nabla \cdot \left(\frac{\mu_T}{\sigma_K} \nabla K \right) + P_K - \beta^* \rho_f K \tag{16}$$

$$\frac{\partial \omega}{\partial t} + u_f \cdot \nabla \omega = \nabla \cdot \left(\frac{\mu_T}{\sigma_\omega} \nabla \omega \right) + \alpha \frac{\omega}{k} P_k - \beta \rho_f \omega \tag{17}$$

where

$$\mu_T = \frac{\rho_f K}{\omega} \tag{18}$$

$$P_k = \mu_T \left[\nabla u_f \cdot \left(\nabla u_f + (\nabla u_f)^T \right) \right] \tag{19}$$

α, σ_K, σ_ω, β, and β^* are constants and are defined as below:

$$\alpha = \frac{3}{25}, \sigma_K = \sigma_\omega = \frac{1}{2}, \beta = \frac{3}{125}, \text{and } \beta^* = \frac{9}{100}$$

2.3.3. Boundary conditions

The following boundary conditions were considered to simulate the comprehensive 3D models:

$$\text{At the inlet}, T = T_i \tag{20}$$

$$\text{At the outlet}, P = 0 \tag{21}$$

$$\text{At the wall } u = v = w \text{ and is considered as non} - \text{slip}. \tag{22}$$

The boundary condition at the layers where conjugate heat transfer occurs between solid and fluid (transferring heat to the water circulating in the copper tube) is solved as [19,23,40,58]:

$$k_S \partial T_s / \partial n = - k_f \partial T_f / \partial n \tag{23}$$

where k_S, k_f, T_s, T_f and $\boldsymbol{n}$ denote the solid thermal conductivity, the fluid thermal conductivity, the solid temperature, the fluid temperature, and the normal vector toward the exterior, respectively.

For thermal insulation domains (collector sides and back), the following equation is considered:

$$-\boldsymbol{n}.q = 0 \tag{24}$$

Here, q is the conductive heat flux.

The incident solar irradiance (q_0) to the PV panel is considered a general heat flux. The following equation is used in the heat flux

Fig. 4. PV/T collectors mesh using a user-controlled mesh sequence in COMSOL software.

interface in COMSOL:

$$-\boldsymbol{n}.q = q_0 \tag{25}$$

In this study, surface-to-ambient radiation accounts for radiation from the PV panel surface (glass) to the ambient and is calculated by:

$$-\boldsymbol{n}.q = \varepsilon\sigma\left(T_{amb}^4 - T^4\right) \tag{26}$$

Here, ε, σ, and T_{amb} represent surface emissivity, the Stefan-Boltzmann constant, and ambient air temperature, respectively.

2.3.4. Mesh generation

Mesh generation for the designed PV/T collectors was accomplished utilizing a user-controlled mesh sequence setting in COMSOL software. All domains were meshed using the free tetrahedral mesh setting with a fine size to produce an accurate heat transfer model and reach more precise results. Fig. 4 depicts the PV/T modules' mesh generation in COMSOL.

3. Results and discussion

3.1. Mass flow rate impact on PV/T performance

Mass flow rate ($\dot{m}$) is a crucial parameter that has a direct impact on determining the performance of a PV/T system, and an increase in $\dot{m}$ enhances the HT rate from the PV module into the working fluid, resulting in higher η_{th}. Numerical and experimental findings demonstrate that at a fixed solar irradiance level, $\dot{m}$ rises from 0.01 to 0.04 kg/s, and η_{th} exhibits an upward trend for all PV/T designs with different cross-sections. Although thermal performance improves as $\dot{m}$ increases from 0.01 to 0.04 kg/s, it subsequently levels off and declines at $\dot{m} = 0.05$ kg/s for all cross-sections. This is because at higher $\dot{m}$, the cooling fluid exits the collector tube before the heat exchange is complete, leading to a lower heat dissipation rate from the solar module.

The results indicate that $\dot{m} = 0.04$ kg/s is the optimal $\dot{m}$, providing the most efficient cross-section systems. Fig. 5 shows how $\dot{m}$ influences the PV/Ts' thermal performance numerically and experimentally with a fixed solar irradiance (I = 1000 W/m^2). The elliptical cross-sectional absorber tube (type A) PV/T collector achieved the maximum heat gain and η_{th} values, with numerical and experimental results of 220.38 W, 217.34 W, 64.9 %, and 63.6 %, respectively.

The obtained data reveal that both current and voltage increase as $\dot{m}$ changes from 0.01 to 0.04 kg/s at a constant I, improving P_{max} and η_{el} for all PV/T collectors. This increase can be attributed to the fact that at a higher $\dot{m}$, more heat accumulates and transfers from the PV module surface to the thermal collector absorber tube, resulting in better electrical performance. Fig. 6 displays how P_{max} and η_{el} are affected by the amount of $\dot{m}$ for all PV/T collectors at $I = 1000$ W/m^2. The thermal collector absorber tube with the elliptical cross-section (type A), achieved the highest P_{max} and η_{el}, with values of 39.5 W, 29.2 W, 11.69 %, and 8.64 %, respectively, numerically and

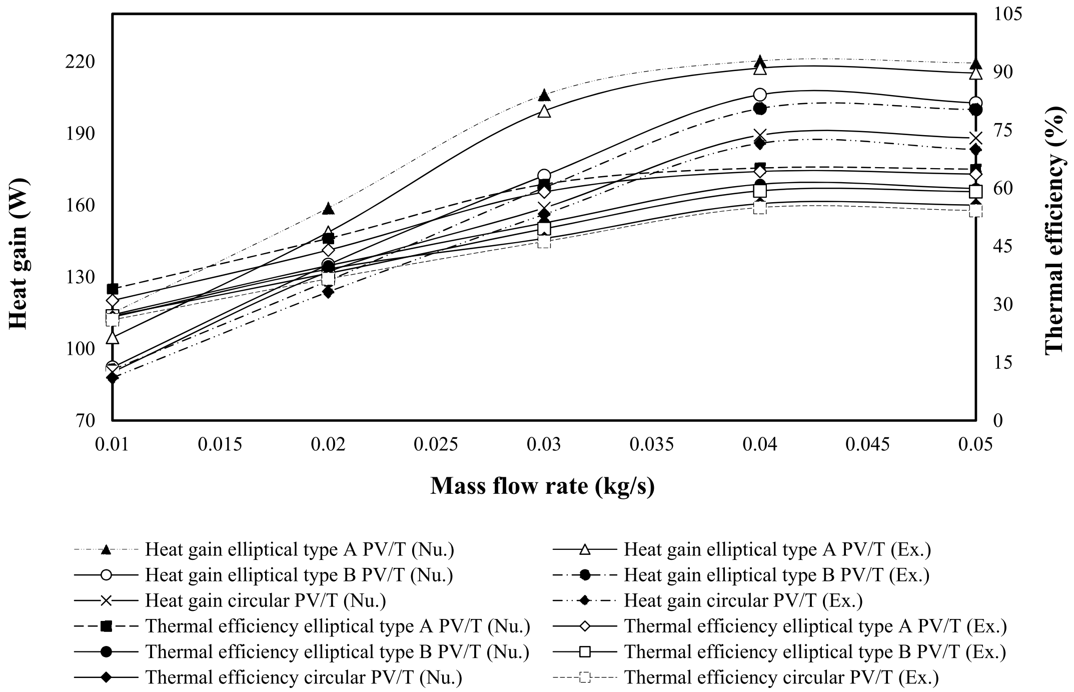

Fig. 5. Heat gain and thermal efficiency vs. $\dot{m}$ at I = 1000 W/m^2.

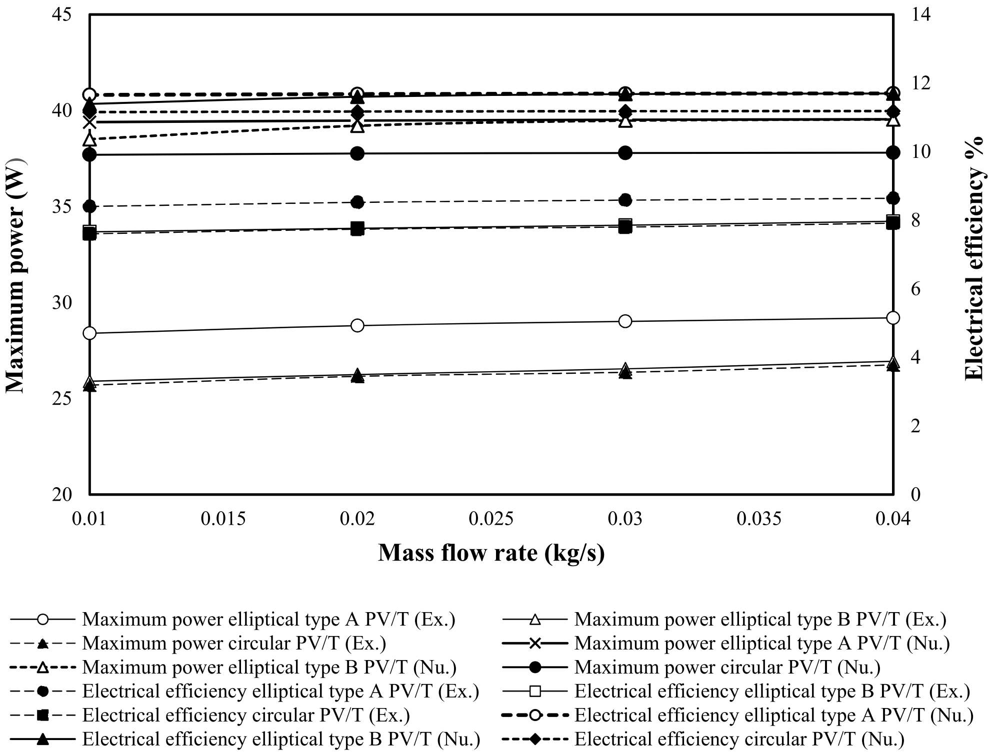

Fig. 6. Maximum power and electrical efficiency vs. $\dot{m}$ at $I = 1000$ W/m^2.

experimentally, at the optimal mass flow rate.

3.2. Temperature effect on PV/T performance

Fig. 7(a)–(d) shows the 3D simulation of PV/T collectors and conventional PV module surface temperature distribution at the optimal mass flow rate and $I = 1000$ W/m^2. It is evident that, due to the cooling effect of water, all PV/T collectors with different absorber tube cross-sections achieved lower surface temperatures than the conventional PV module. The lowest average surface temperature belongs to the elliptical (type A) PV/T collector, which averages 20 °C less than the conventional PV module (Fig. 7(a)).

Fig. 8 shows the relationship among the average cell temperature, $\dot{m}$, and T_o-T_i of the PV/T collectors at $I = 1000$ W/m^2. As $\dot{m}$ increases at a constant solar irradiance, numerical and experimental results indicate a reduction in the average cell temperature for all collector designs. This improved heat dissipation from the PV module surface at higher flow rates results in a lower temperature. Numerically, the lowest average surface temperatures of 66.91 °C, 67.95 °C, and 73.87 °C are obtained for the elliptical type A, elliptical type B, and circular PV/T collectors, respectively.

T_o-T_i also exhibits a similar trend. T_o-T_i decreases with increasing flow rates in numerical and experimental cases for all PV/T collectors. This can be explained by the fact that at higher $\dot{m}$ due to a larger volume of water, the necessary HT from the PV module surface to water occurs in a shorter time, decreasing T_o-T_i. However, T_o-T_i is the highest at the minimum $\dot{m}$ (0.01 kg/s). Nevertheless, at lower flow rates, the systems require longer to reach the necessary heat transfer and remove heat from the PV module surface. Therefore, the greatest amount of T_o-T_i at lower flow rates does not necessarily lead to higher thermal efficiency.

The average cell temperature directly impacts a PV module's electrical efficiency. As mentioned in the previous section, the average cell temperature drops as the flowing working fluid collects more heat from the PV/T collector's surface. This reduction is more pronounced at higher water flow rates, increasing electrical efficiency for all PV/T collectors. As the average cell temperature decreases from 68.12 to 66.95 °C, 71.05 to 70.49 °C, and 74.35 to 73.92 °C, the electrical efficiency numerically and experimentally increases from 11.65 to 11.69 %, 8.4–8.64 %, 11.39–11.62 %, 7.66–7.97 %, 11.15–11.18 %, and 7.6–7.91 % for elliptical (type A), elliptical (type B), and circular absorber tube PV/T systems, respectively. These results are depicted in Fig. 9 for experimental tests.

3.3. Solar irradiance impact on PV/T performance

The numerical and experimental results reveal that increasing I from 400 to 1000 W/m^2 leads to an upward trend in the PV/Ts thermal performance at a constant $\dot{m}$. Fig. 10 illustrates PV/Ts' heat gain and thermal efficiency at 400, 600, 800, and 1000 W/m^2 solar irradiance levels at the optimal mass flow rate. The elliptical (type A) cross-sectional absorber tube PV/T collector achieves the greatest thermal efficiency, with 64.9 % and 63.6 % values for numerical and experimental cases, respectively, at $I = 1000$ W/m^2.

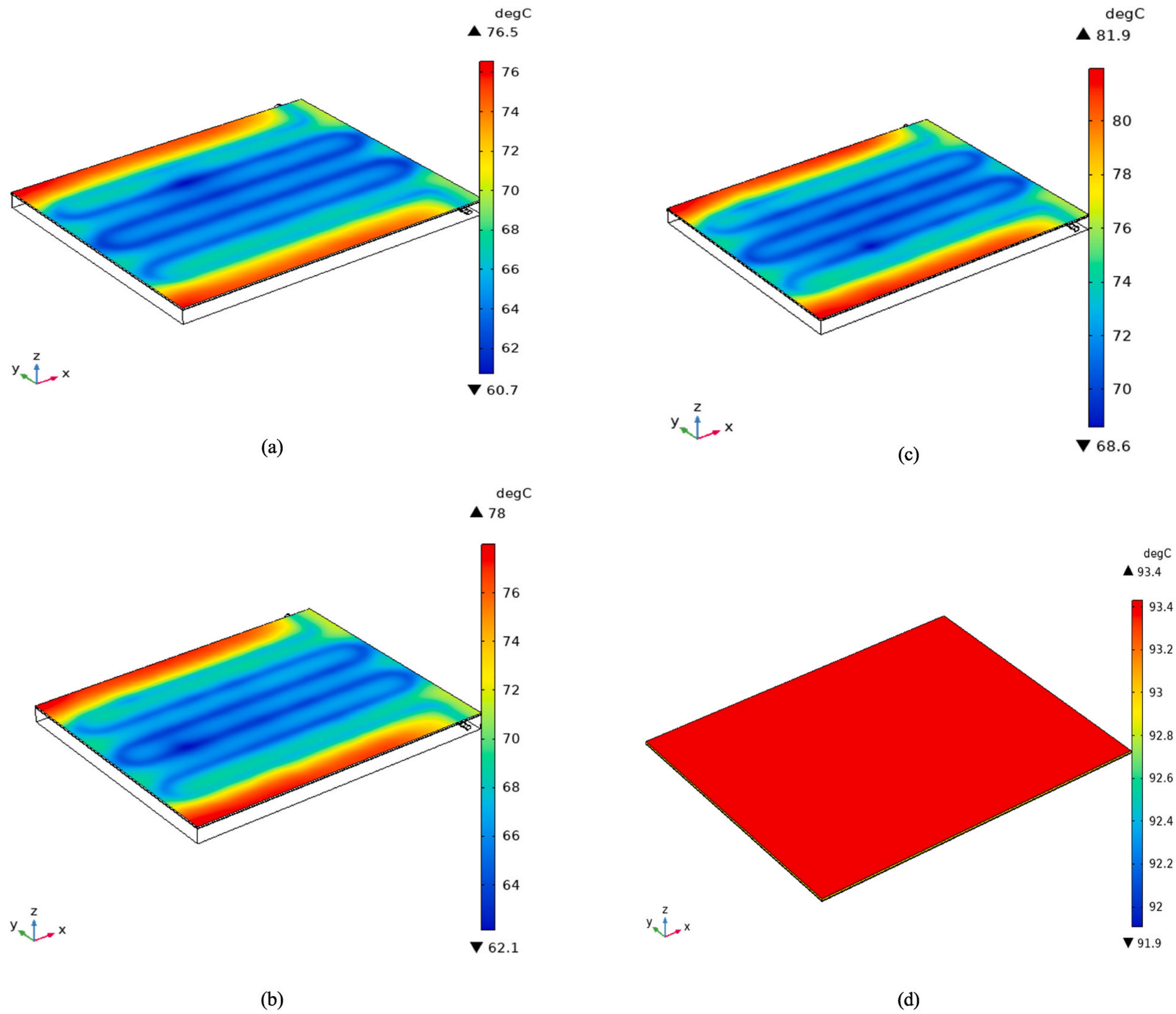

Fig. 7. 3D plot of PV/T collectors and the conventional PV module surface temperature at the optimal mass flow rate and $I = 1000$ W/m^2: (a) elliptical (type A), (b) elliptical (type B), (c) circular cross-sectional absorber tube collector, and (d) conventional PV module.

The findings indicate that while current, voltage, and maximum power increase with rising I from 400 to 1000 W/m^2, electrical efficiency decreases for all PV/T systems and the conventional PV module. This decline in η_{el} can be attributed to higher cell temperatures at higher solar irradiation levels. As I rise from 400 to 1000 W/m^2, η_{el}, numerically and experimentally drops from 13.56 to 11.69 %,10.34 to 8.64 %, 13.45 to 11.56 %, 8.84 to 7.97 %, 8.68 to 7.91 %, 13.19 to 11.18 %, and 7.47 %–7.07 % for elliptical (type A), elliptical (type B), and circular PV/T collectors plus the conventional PV module, respectively. Due to the lack of a cooling effect from water, the conventional PV module numerically and experimentally exhibits the lowest electrical performance, with 32.7 W and 23.9 W of maximum power and 9.7 % and 7.07 % of electrical efficiency at $I = 1000$ W/m^2, respectively. Fig. 11 reveals how solar irradiance values impact the electrical performance of the conventional PV module and the PV/T designs at the optimal mass flow rate.

3.4. Reynolds number effect on PV/T performance

Fig. 12 represents how the Re directly affects the PV/T collectors' thermal efficiency. As the $\dot{m}$ changes from 0.01 to 0.04 kg/s, η_{th} rises by approximately 30 % when transitioning from laminar to turbulent flow for all cross-sections. This improvement in thermal efficiency is primarily attributed to the transition from laminar to turbulent flow, which significantly enhances heat transfer. The highest thermal efficiency values are achieved at the maximum Reynolds numbers for all cross-sections at the optimal $\dot{m}$ ($\dot{m} = 0.04$ kg/s) and $I = 1000$ W/m^2. Specifically, the elliptical type A cross-sectional absorber tube PV/T collector reaches the highest Reynolds number value of 5502.92, while the Reynolds number values for the elliptical type B and circular cross-sectional solar thermal collectors are 4813.12 and 3768.89, respectively, at the optimal mass flow rate.

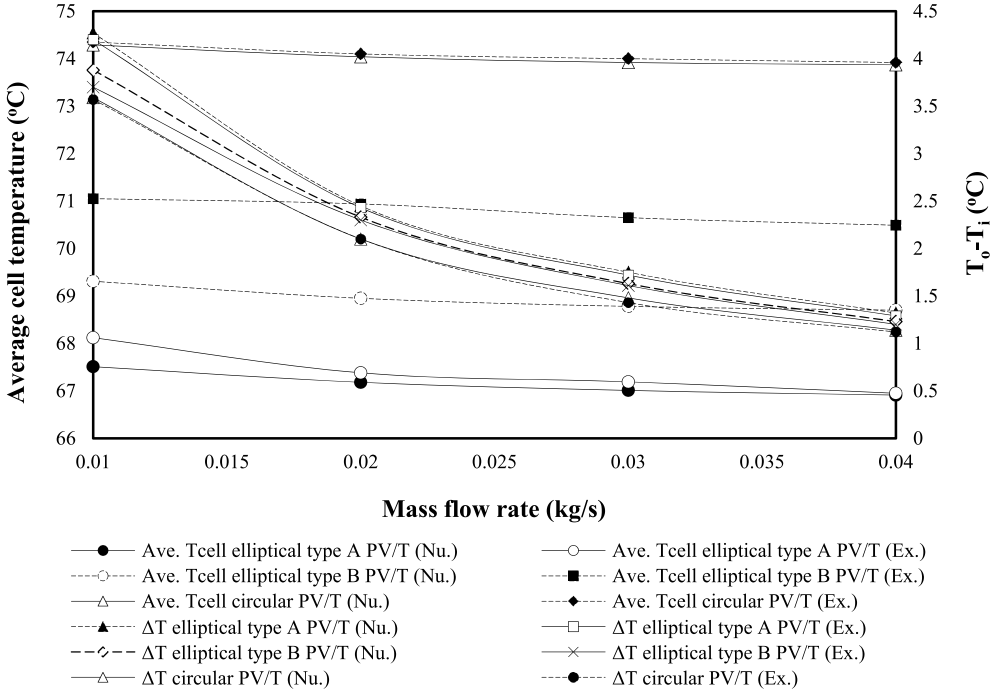

Fig. 8. The average cell temperature and (T_o-T_i) vs. $\dot{m}$ at $I = 1000$ W/m^2.

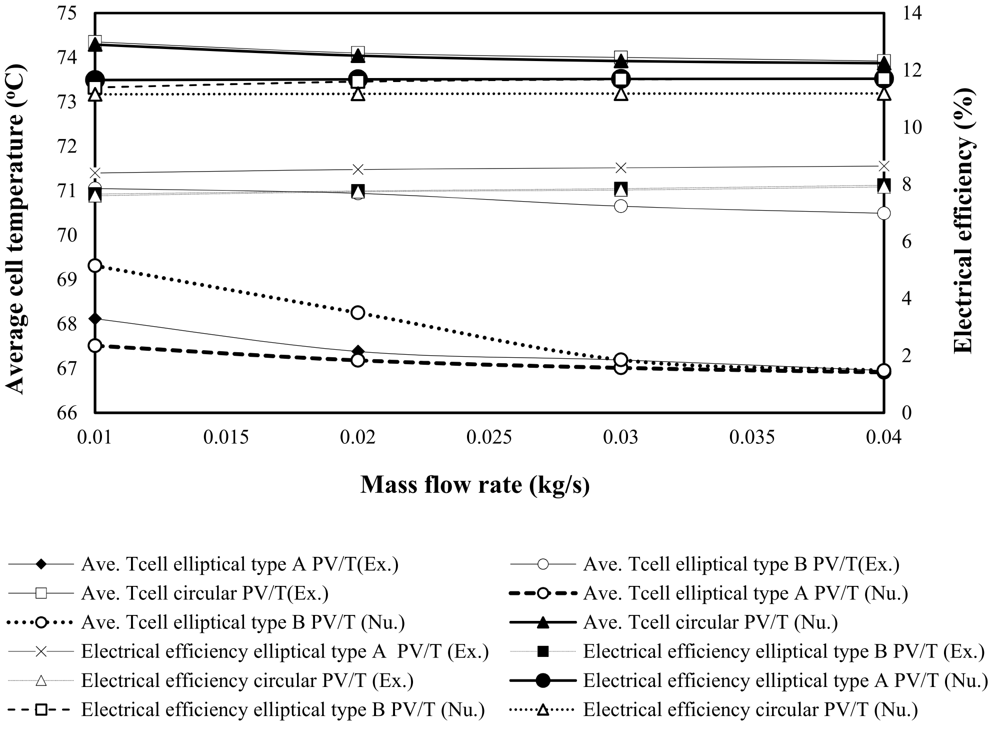

Fig. 9. Effect of the average cell temperature on electrical efficiency vs. $\dot{m}$ at $I = 1000$ W/m.^{2}.

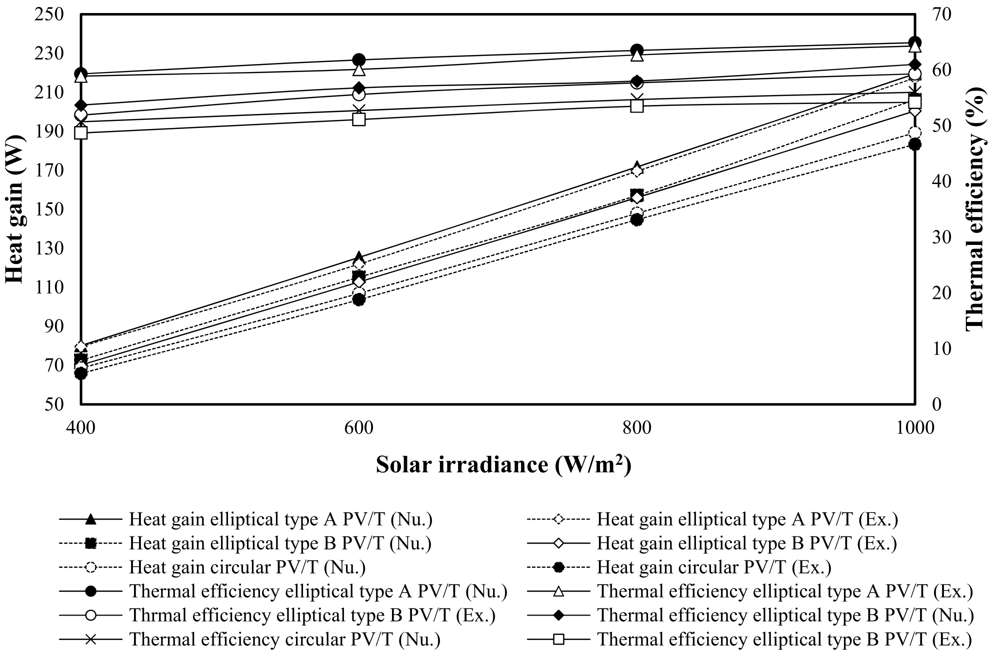

Fig. 10. Heat gain and thermal efficiency vs. I at the optimal $\dot{m}$.

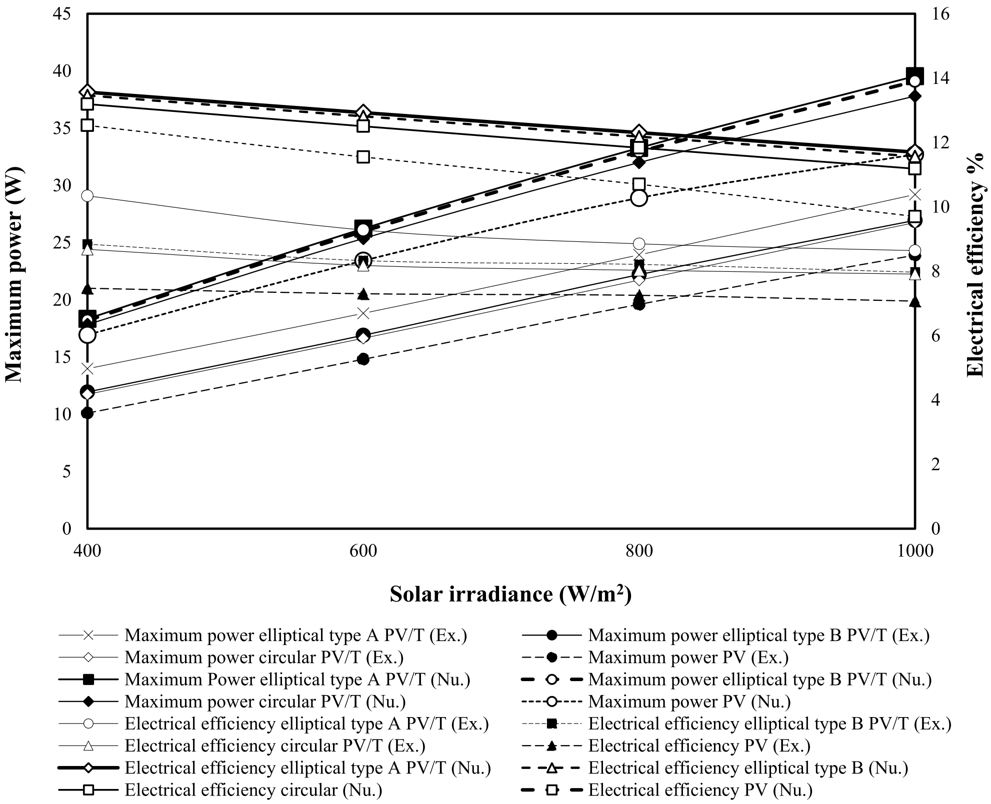

Fig. 11. Maximum power and electrical efficiency vs. I at the optimal $\dot{m}$.

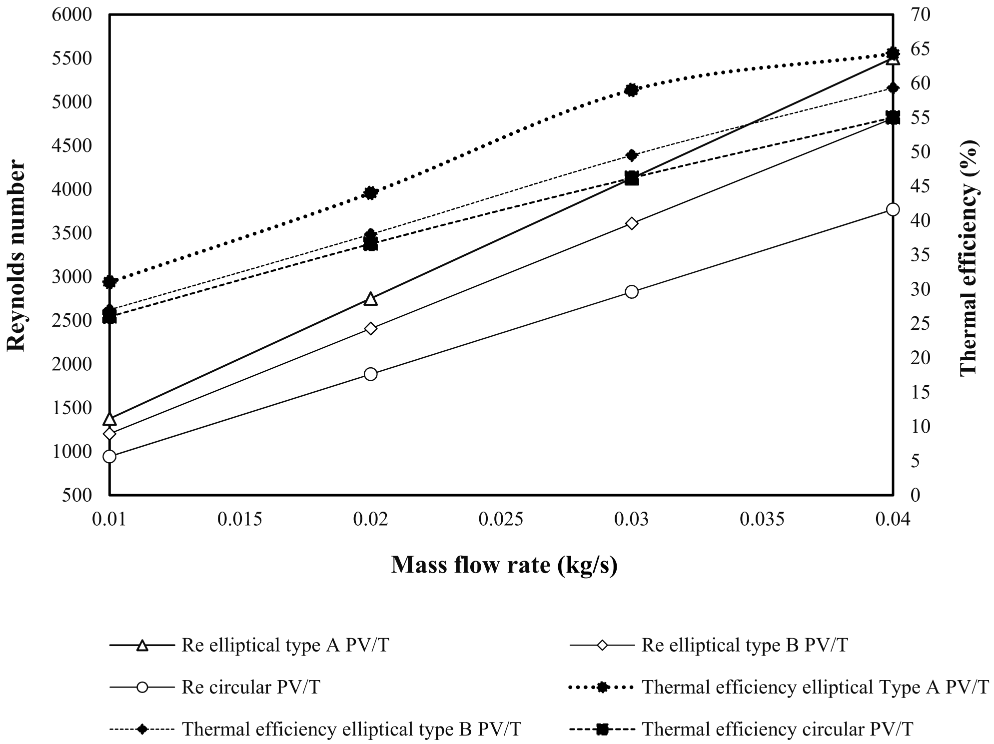

Fig. 12. Effect of Reynolds number on thermal efficiency vs. $\dot{m}$ at $I = 1000$ W/m^2.

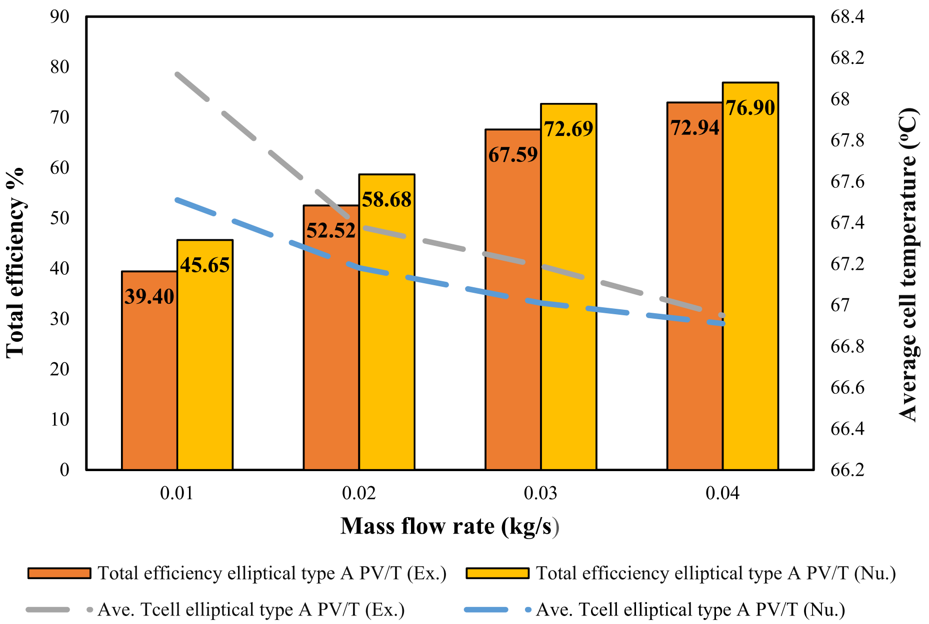

Fig. 13. Elliptical type A PV/T collector's total efficiency vs. the mass flow rate and average cell temperature at $I = 1000$ W/m^2.

3.5. *Total efficiency of PV/T collectors*

Figs. 13–15 demonstrate the PV/T collectors' total efficiency against $\dot{m}$ and average cell temperatture. The elliptical PV/T collector (type A) with the lowest hydraulic diameter exhibited the best performance, achieving the highest total efficiency of 76.9 % and 72.94 % numerically and experimentally, respectively, at the optimal mass flow rate and $I = 1000$ W/m^2. In contrast, the circular PV/T collector with the highest hydraulic diameter yielded the lowest total efficiency values, numerically and experimentally, at 67.18 %

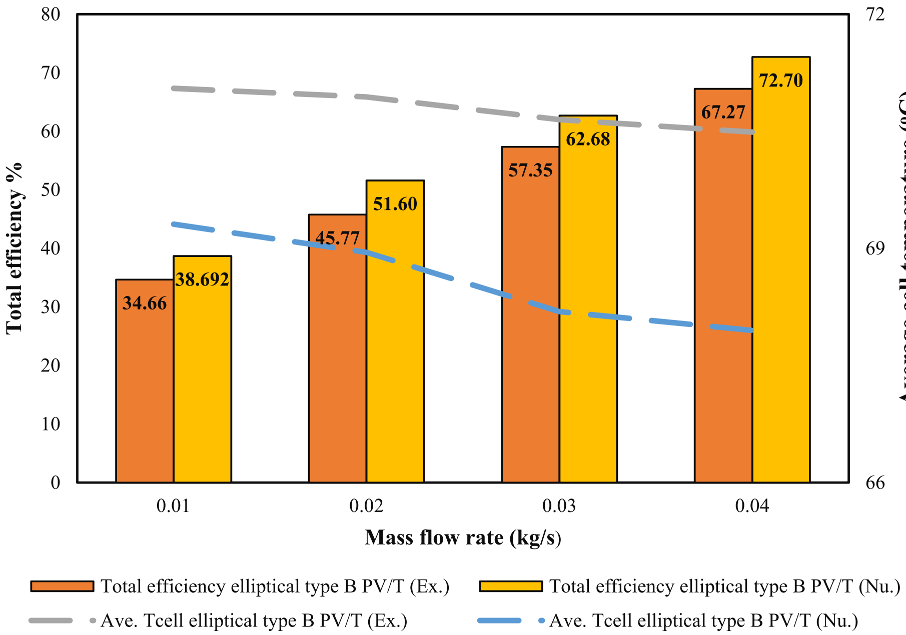

Fig. 14. Elliptical type B PV/T collector' total efficiency vs. the mass flow rate and average cell temperature at $I = 1000$ W/m^2.

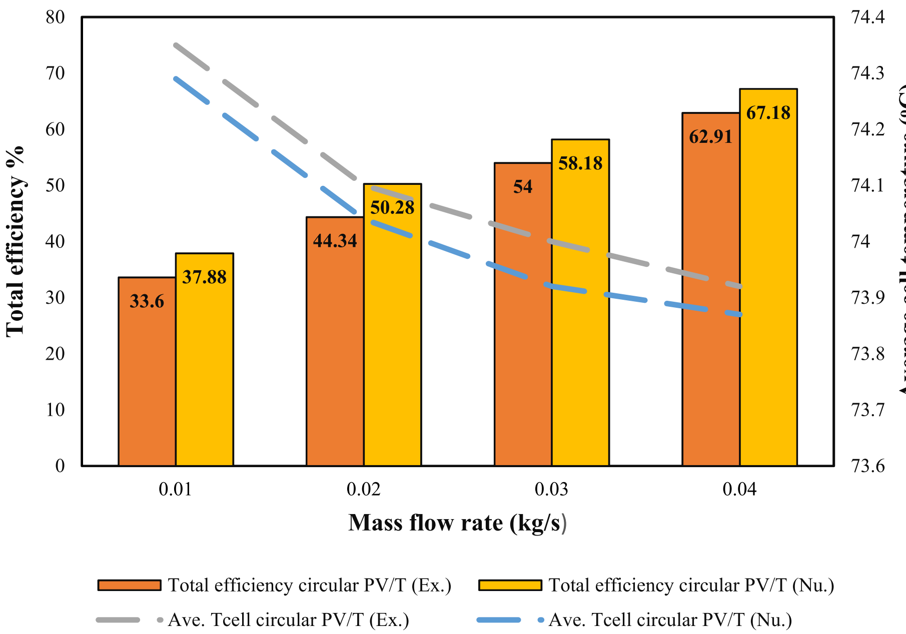

Fig. 15. Circular PV/T collector's total efficiency vs. the mass flow rate and average cell temperature at $I = 1000$ W/m^2.

and 62.91 %, respectively.

4. Conclusions

We have conducted numerical and experimental investigations to assess and compare the performance of serpentine WPV/T collectors with elliptical, and circular cross-sectional absorber tubes, along with a conventional PV module. Numerical simulations were performed using COMSOL software, and indoor tests were conducted to validate the numerical results. From the results, the subsequent deductions can be made:

- Although there was a fair agreement between numerical and experimental results, any discrepancies between the numerical and experimental values were rooted in uncontrollable ambient variables, such as inaccuracies in mass flow rate or ambient temperature during data collection.
- It was found that $\dot{m} = 0.04$ kg/s is the optimal choice, resulting in the most efficient systems for all cross-sections, both numerically and experimentally.
- Increasing $\dot{m}$ from 0.01 to 0.04 kg/s at a constant I, increased heat gain, thermal efficiency, maximum power, electrical efficiency, Reynolds number, and total efficiency for all PV/T collectors with different cross-sections. However, the average cell temperature and (T_o-T_i) showed a downward trend.
- The highest heat gain values, both numerical and experimental, were achieved by the elliptical (type A) PV/T collector, 220.38 W and 217.34 W, respectively, under turbulent flow conditions ($Re = 5502.92$) at the optimal mass flow rate and $I = 1000$ W/m^2. As a result, the maximum η_{th} reached 65.2 % and 64.3 %, numerically and experimentally, respectively, under turbulent flow for the elliptical solar thermal collector.
- As I increased from 400 to 1000 W/m^2, electrical efficiency dropped by 1.87 %, 1.7 %, 1.78 %, 0.88 %, and 2 % and 0.77 % for elliptical (type A), elliptical (type B), and circular PV/T absorber tubes, numerically and experimentally, respectively. The conventional PV module's electrical efficiency numerically and experimentally declined by 2.8 % and 0.4 % within the same range.
- At the optimal mass flow rate and 1000 W/m^2 irradiance, the elliptical PV/T collector absorber tube with the least hydraulic diameter, numerically and experimentally achieved the highest maximum power and electrical efficiency at 39.54 W, 29.2 W, 11.69 %, and 8.64 %, respectively. These values were greater than those of the conventional PV module, which had the minimum power and electrical efficiency of 32.7 W, 23.9 W, 9.7 % and 7.07 %, numerically and experimentally, respectively.
- The elliptical (type A) PV/T collector demonstrated superior performance, attaining the highest total efficiency of 76.9 % numerically and 72.94 % experimentally at the optimal mass flow rate and an irradiance of 1000 W/m^2. Conversely, the circular PV/T collector with the highest hydraulic diameter exhibited the lowest total efficiency values, recording 67.18 % numerically and 62.91 % experimentally.
- It was concluded that among tubes fabricated with different cross-sections but the same perimeter, the cross-section with the smallest hydraulic diameter (7.8 mm for the elliptical (type A) design) exhibited the highest heat transfer characteristics when compared to cross-sections with larger hydraulic diameters (10.4 mm for circular and 9.8 mm for elliptical (type B) designs).
- According to the findings of this innovative research, optimizing the absorber tube's cross-sectional configuration and hydraulic diameter presents an opportunity to enhance the HT properties of the PV/T system, ultimately leading to an increase in the system's total efficiency. Additionally, the improved design facilitates progress in future studies and has the potential to be developed for both residential and commercial applications.

CRediT authorship contribution statement

Shirin Rostami: Writing – Conceptualization, Data curation, Investigation, Methodology, Validation, Writing – original draft, Writing – review & editing. **Adnan Ibrahim:** Conceptualization, Funding acquisition, Project administration, Supervision, Validation, Writing – review & editing. **Amir Aziat Ishak:** Conceptualization, Funding acquisition, Project administration, Supervision, Validation, Writing – review & editing. **Ahmad Fazlizan:** Conceptualization, Data curation, Investigation, Methodology, Validation. **Ahmad Fudholi:** Conceptualization, Data curation, Investigation, Methodology, Validation. **Kamaruzzaman Sopian:** Conceptualization, Data curation, Investigation, Methodology, Validation. **Alireza Dehghani-Sanij:** Data curation, Methodology, Supervision, Validation, Writing – review & editing. **Amin Shahsavar:** Data curation, Methodology, Supervision, Validation, Writing – review & editing. **Khaled M. Al-Aribe:** Funding acquisition, Project administration, Supervision, Validation, Writing – review & editing.

Declaration of competing interest

The authors declare that they have no known competing financial interests or personal relationships that could have appeared to influence the work reported in this paper.

Many thanks and regards.

Nomenclature

$2a$	Major axis (m)	T_{ref}	Constant = 25 (°C)
A_c	PV/T collector area (m^2)	u_f	Fluid velocity vector (m/s)
A_{tc}	Tube cross-section area (m^2)	u_s	Translational motion velocity vector (m/s)
$2b$	Minor axis (m)	V_f	Fluid velocity (m/s)
C_{pf}	Specific heat capacity of fluid phase (J/kg.K)	V_{mp}	Maximum power voltage (V)
C_{sf}	Specific heat capacity of solid phase (J/kg.K)	V_{oc}	Open-circuit voltage (V)
D_h	Hydraulic diameter (m)	u, v, w	Fluid velocity vector's components (m/s)
$\boldsymbol{F}$	Volume force (N/m^3)	**Greek Symbols**	
I	Solar irradiance (W/m^2)	α	Constant $= \frac{3}{25}$

(continued on next page)

(*continued*)

I	Moment of inertia (kg/m^2)	β	Constant $= \frac{3}{125}$
I_{mp}	Maximum power current (A)	β^*	Constant $= \frac{9}{100}$
I_{sc}	Short-circuit current (A)	β_{cell}	Temperature coefficient of PV cell (1/K)
k	Thermal conductivity (W/m.K)	η_{el}	Electrical efficiency
K	The turbulent kinetic energy (J/kg)	η_{ref}	Reference efficiency
k_f	Thermal conductivity, fluid phase (W/m.K)	η_{th}	Thermal efficiency
k_s	Thermal conductivity, solid phase (W/m.K)	η_{total}	Total efficiency
$\dot{m}$	Mass flow rate (kg/s)	μ_{df}	Fluid dynamic viscosity (m^2/s)
$\boldsymbol{n}$	Normal vector toward exterior	μ_{eff}	Fluid effective viscosity (m^2/s)
k_f	Thermal conductivity, fluid phase (W/m.K)	μ_T	Fluid turbulent viscosity (m^2/s)
k_s	Thermal conductivity, solid phase (W/m.K)	T_s	Solid temperature (°C)
$\dot{m}$	Mass flow rate (kg/s)	T_o	Fluid outlet temperature (°C)
$\boldsymbol{n}$	Normal vector toward exterior	∇	Vector differential operator
P	Pressure (Pa)	ε	Surface emissivity
P_c	Perimeter of tube cross-section (m)	ρ_f	Fluid density (kg/m^3)
P_{max}	Maximum power (W)	ρ_s	Solid density (kg/m^3)
q	Conductive heat flux (W/m^2)	σ	Stefan-Boltzmann constant (W/m^2.K^4)
q_0	Inward heat flux (W/m^2)	σ_K	Constant $= \frac{1}{2}$
Q_f	Heat sources other than viscous dissipation (W/m^3)	σ_ω	Constant $= \frac{1}{2}$
Q_P	Work done by pressure changes (W/m^3)	ω	Specific dissipation rate (1/s)
Q_s	Additional heat sources (W/m^3)	**Abbreviations**	
Q_{ted}	Thermo-elastic damping (W/m^3)	EVA	Ethylene vinyl acetate
Q_u	Useful energy gain (W)	FEM	Finite element method
$Q_{\vartheta d}$	Heat sources via viscous dissipation (W/m^3)	HT	Heat transfer
Re	Reynolds number	LPM	Liters per minute
T	Temperature (°C)	PV	Photovoltaic
T_{amb}	Ambient air temperature (°C)	PV/T	Photovoltaic/thermal
T_{Ave}	Average cell temperature (°C)	RANS	Reynolds-Averaged Navier-Stokes equations
T_i	Fluid inlet temperature (°C)	WPV/T	Water-based photovoltaic/thermal
T_f	Fluid temperature (°C)	3D	Three-dimensional

Data availability

Data will be made available on request.

References

[1] S. Abdul-Ganiyu, D.A. Quansah, E.W. Ramde, R. Seidu, M.S. Adaramola, Study effect of flow rate on flat-plate water-based photovoltaic-thermal (PVT) system performance by analytical technique, J. Clean. Prod. 321 (2021) 128985, https://doi.org/10.1016/j.jclepro.2021.128985.

[2] F. Sarhaddi, S. Farahat, H. Ajam, A. Behzadmehr, M. Mahdavi Adeli, An improved thermal and electrical model for a solar photovoltaic thermal (PV/T) air collector, Appl. Energy 87 (2010) 2328–2339, https://doi.org/10.1016/j.apenergy.2010.01.001.

[3] Z. Ul Abdin, A. Rachid, A survey on applications of hybrid PV/T panels, Energies 14 (2021) 1205, https://doi.org/10.3390/en14041205.

[4] S. Abdul-Ganiyu, D.A. Quansah, E.W. Ramde, R. Seidu, M.S. Adaramola, Investigation of solar photovoltaic-thermal (PVT) and solar photovoltaic (PV) performance: a case study in Ghana, Energies 13 (2020) 2701, https://doi.org/10.3390/en13112701.

[5] A. Faddouli, M. Hajji, S. Fadili, B. Hartiti, H. Labrim, A. Habchi, A comprehensive review of solar, thermal, photovoltaic, and thermoelectric hybrid systems for heating and power generation, Int. J. Green Energy 21 (2023) 413–447, https://doi.org/10.1080/15435075.2023.2196340.

[6] L. Kegui, Y. Qiongwan, Z. Bin, P. Gang, Performance analysis of a novel PV/T hybrid system based on spectral beam splitting, Renew. Energy 207 (2023) 398–406, https://doi.org/10.1016/j.renene.2023.03.007.

[7] A. Atiz, M. Erden, M. Karakilcik, Hydrogen production of flat plate solar collectors integrated with photovoltaic thermal panels, Int. J. Hydrog. Energy 2 (2024) 1408–1424, https://doi.org/10.1016/j.ijhydene.2023.08.302.

[8] M. Amar, N. Akram, G.Q. Chaudhary, S.N. Kazi, M.E.M. Soudagar, N.M. Mubarak, Energy, exergy and economic (3E) analysis of flat-plate solar collector using novel environmental friendly nanofluid, Sci. Rep. 13 (2023) 411, https://doi.org/10.1038/s41598-023-27491-w.

[9] V.K. Gupta, S. Kumar, R. Kukreja, N. Chander, Experimental thermal performance investigation of a direct absorption solar collector using hybrid nanofluid of gold nanoparticles with natural extract of Azadirachta Indica leaves, Renew. Energy 202 (2023) 1021–1031, https://doi.org/10.1016/j.renene.2022.12.014.

[10] A. Saber, S.S. Hind, M.A. Abdelrahman, Numerical study with eco-exergy analysis and sustainability assessment for a stand-alone nanofluid PV/T, TSEP 24 (2021) 100931, https://doi.org/10.1016/j.tsep.2021.100931.

[11] S.H. Rostami, A.S. Abd Hamid, K. Sopian, H. Jarimi, A. Bassim, A. Ibrahim, Heat transfer analysis of the flat plate solar thermal collectors with elliptical and circular serpentine tubes, Appl. Sci. 12 (2022) 4519, https://doi.org/10.3390/app12094519.

[12] A. Shahsavar, A.H.A. Alwaeli, N. Azimi, Sh Rostami, K. Sopian, M. Arıcı, P. Estellé, S. Nižetić, A. Kasaeian, H.M. Ali, Zh Ma, M. Afrand, Exergy studies in water-based and nanofluid-based photovoltaic/thermal collectors: status and prospects, Renew. Sustain. Energy Rev. 168 (2022) 112740, https://doi.org/10.1016/j.rser.2022.112740.

[13] A.L. Abdullah, S. Misha, N. Tamaldin, M.A.M. Rosli, F.A. Sachit, A Review: parameters affecting the PVT collector performance on the thermal, electrical, and overall efficiency of PVT system, J. Adv. Res. Fluid Mech. 60 (2019) 191–232.

[14] B. Yan, W. Qiuxuan, X. Chi, C. Wu, P. Luo, Y. Luo, Numerical and experimental investigation of photovoltaic/thermal systems: parameter analysis and determination of optimum flow, Sustain. 14 (2022) 10156, https://doi.org/10.3390/su141610156.

[15] T.B. Korkut, A. Gören, A. Rachid, Numerical and experimental study of a PVT water system under daily weather conditions, Energies 15 (2022) 6538, https://doi.org/10.3390/en15186538.
[16] J.H. Kim, J.T. Kim, Comparison of electrical and thermal performances of glazed and unglazed PVT collectors, Int. J. Photoenergy 2012 (2012) 1–7, https://doi.org/10.1155/2012/957847.
[17] K. Arash, M. Tao, H. Yang, Evaluation of various collector configurations for a photovoltaic thermal system to achieve high performance, low cost, and lightweight, Appl. Energy 357 (2024) 122422, https://doi.org/10.1016/j.apenergy.2023.122422.
[18] M.M.S. Dezfouli, A.R. Dehghani-Sanij, K. Kadir, K. Sopian, Development and life cycle cost analysis of a solar hybrid HVAC system for use in buildings in tropical climates, Sustain. Energy Technol. Assess. 57 (2023) 103143, https://doi.org/10.1016/j.seta.2023.103143.
[19] H. Fayaz, N.A. Rahim, M. Hasanuzzaman, R. Nasrin, A. Rivai, Numerical and experimental investigation of the effect of operating conditions on performance of PVT and PVT-PCM, Renew. Energy 143 (2019) 827–841, https://doi.org/10.1016/j.renene.2019.05.041.
[20] W. Pang, Q. Zhang, Y. Cui, L. Zhang, H. Yu, X. Zhang, Numerical simulation and experimental validation of a photovoltaic/thermal system based on a roll-bond aluminum collector, Energy 187 (2019) 115990, https://doi.org/10.1016/j.energy.2019.115990.
[21] R. Nasrin, N.A. Rahim, H. Fayaz, M. Hasanuzzaman, Water/MWCNT nanofluid based cooling system of PVT: experimental and numerical research, Renew. Energy 121 (2018) 286–300, https://doi.org/10.1016/j.renene.2018.01.014.
[22] A. Nahar, M. Hasanuzzaman, Numerical investigation on the effect of different parameters in enhancing heat transfer performance of photovoltaic thermal systems, Renew. Energy 132 (2019) 284–295, https://doi.org/10.1016/j.renene.2018.08.008.
[23] F.T. Zohora, R. Nasrin, A numerical analogy of improving efficiency for the PVT system in Bangladesh, Int. J. Photoenergy 2022 (2022) 1–21, https://doi.org/10.1155/2022/1901925.
[24] A.M. Bassam, K. Sopian, A. Ibrahim, A.B. Al-Aasam, M. Dayer, Experimental analysis of photovoltaic thermal collector (PVT) with nano PCM and micro-fins tube counterclockwise twisted tape nanofluid, Case Stud. Therm. Eng. 45 (2023) 102883, https://doi.org/10.1016/j.csite.2023.102883.
[25] R. Oussama, L. Bilal, L. Ravita, K. Tarik, S. Tareq, J. Abdelmajid, Numerical investigations of concentrated photovoltaic thermal system integrated with thermoelectric power generator and phase change material, J. Energy Storage 62 (2023) 106820, https://doi.org/10.1016/j.est.2023.106820.
[26] W. Pang, Y. Cui, Q. Zhang, H. Yu, L. Zhang, H. Yan, Experimental effect of high mass flow rate and volume cooling on performance of a water-type PV/T collector, Sol. Energy 188 (2019) 1360–1368, https://doi.org/10.1016/j.solener.2019.07.024.
[27] S.S. Park, Y.J. Kim, E.C. Kang, E.J. Lee, E. Entchev, Numerical investigations of a solar energy heat transfer performances with experimental validations in a water-based serpentine photovoltaic-thermal (PVT) collector, J. Therm. Anal. Calorim. 148 (2023) 2149–2169, https://doi.org/10.1007/s10973-022-11861-z.
[28] A.L. Abdullah, S. Misha, N. Tamaldin, M.A.M. Rosli, F.A. Sachit, Theoretical study and indoor experimental validation of performance of the new photovoltaic thermal solar collector (PVT) based water system, Case Stud. Therm. Eng. 18 (2020) 100595, https://doi.org/10.1016/j.csite.2020.100595.
[29] N.S.B. Rukman, A. Fudholi, W. Nuriana, G.H. Pikra, H. Sudibyo, R.A. Subekti, Thermal efficiencies of photovoltaic thermal (PVT) with Bi-fluid cooling system, Int. J. Heat Technol. 40 (2) (2022) 423–428, https://doi.org/10.18280/ijht.400209.
[30] M. Fterich, H. Chouikhi, S. Sandoval-Torres, H. Bentaher, A. Elloumi, A. Maalej, Numerical simulation and experimental characterization of the heat transfer in a PV/T air collector prototype, Case Stud. Therm. Eng. 27 (2021) 101209, https://doi.org/10.1016/j.csite.2021.101209.
[31] A. Yogesh, M. Anirudh, G. Atul, P. Gaurak, S.Y. Anil, V. Monika, Performance analysis of photovoltaic thermal air collector having rectangular fins, Mater. Today: Proc. 84 (2023) 6–15, https://doi.org/10.1016/j.matpr.2023.03.787.
[32] Z. Saberi, H. Jarimi, M.H. Hj Jumali, S. Suhendri, S. Riffat, A. Fudholi, Performance assessment of double pass photovoltaic/thermal solar air collector using bifacial PV with CPC and mirror reflector under Malaysian climate, Case Stud. Therm. Eng. 44 (2023) 102811, https://doi.org/10.1016/j.csite.2023.102811.
[33] E. Bisengimana, Y. Yuan, B. Maxime, N. Gaudence, J. Zhou, A review on the influence of the components on the performance of PVT modules, Sol. Energy 2269 (2021) 365–388, https://doi.org/10.1016/j.solener.2021.08.042.
[34] O. Rejeb, H. Dhaou, A. Jemni, A numerical investigation of a photovoltaic thermal (PV/T) collector, Renew. Energy 77 (2015) 43–50, https://doi.org/10.1016/j.renene.2014.12.012.
[35] M. Mourshed, N.I. Masuk, H.Q. Nguyen, B. Shabani, An experimental approach to energy and exergy analyses of a hybrid PV/T system with simultaneous water and air cooling, Energies 15 (2022) 6764, https://doi.org/10.3390/en15186764.
[36] P. Jha, B. Das, R. Gupta, J.D. Mondol, M.A. Ehyaei, Review of recent research on photovoltaic thermal solar collectors, Sol. Energy 257 (2023) 164–195, https://doi.org/10.1016/j.solener.2023.04.004.
[37] A. Allouhi, S.H. Rehman, M.S. Buker, Z. Said, Recent technical approaches for improving energy efficiency and sustainability of PV and PV-T systems: a comprehensive review, Sustain. Energy Technol. Assess. 56 (2023) 103026, https://doi.org/10.1016/j.seta.2023.103026.
[38] T. Maatallah, R. Zachariah, F.G. Al-Amri, Exergo-economic analysis of a serpentine flow type water based photovoltaic thermal system with phase change material (PVT-PCM/water), Sol. Energy 193 (2019) 195–204, https://doi.org/10.1016/j.solener.2019.09.063.
[39] A.H.A. Al-Waeli, K. Sopian, H.A. Kazem, M.T. Chaichan, Photovoltaic/Thermal (PV/T) systems: status and prospects, Renew. Sustain. Energy Rev. 77 (2017) 109–130, https://doi.org/10.1016/j.rser.2017.03.126.
[40] A.K. Azad, S. Parvin, Photovoltaic thermal (PV/T) performance analysis for different flow regimes: a comparative numerical study, Int. J. Thermofluids 18 (2023) 100319, https://doi.org/10.1016/j.ijft.2023.100319.
[41] A.L. Abdullah, S. Misha, N. Tamaldin, M.A.M. Rosli, F.A. Sachit, Photovoltaic thermal/solar (PVT) collector (PVT) system based on fluid absorber design: a review, J. Adv. Res. 48 (2018) 196–208.
[42] A. Nahar, M. Hasanuzzaman, N.A. Rahim, Numerical and experimental investigation on the performance of a photovoltaic thermal collector with parallel plate flow channel under different operating conditions in Malaysia, Sol. Energy 144 (2017) 517–528, https://doi.org/10.1016/j.solener.2017.01.041.
[43] F. Yazdanifard, E. Ebrahimnia-Bajestan, M. Ameri, Investigating the performance of a water-based photovoltaic/thermal (PV/T) collector in laminar and turbulent flow regime, Renew. Energy 99 (2016) 295–306, https://doi.org/10.1016/j.renene.2016.07.004.
[44] H. Jarimi, M.N. Abu Bakar, M. Othman, M. Hj Din, Bi-fluid photovoltaic/thermal (PV/T) solar collector: experimental validation of a 2-D theoretical model, Renew. Energy 85 (2016) 1052–1067, https://doi.org/10.1016/j.renene.2015.07.014.
[45] A.L. Abdullah, S. Misha, N. Tamaldin, M.A.M. Rosli, F.A. Sachit, Theoretical study and indoor experimental validation of performance of the new photovoltaic thermal solar collector (PVT) based water system, Case Stud. Therm. Eng. 18 (2020) 100595, https://doi.org/10.1016/j.csite.2020.100595.
[46] J. Allan, Z. Dehouche, S. Stankovic, M. Lascelle, Performance testing of thermal and photovoltaic thermal solar collectors, Energy Sci. Eng. 3 (2015) 310–326, https://doi.org/10.1002/ese3.75.
[47] S.R. Faysal, I.R.Q. Ovi, A.K.M. Islam, Effect of aspect ratio on convective heat transfer for flat cross section using nanofluid, 7th BSME Int. Conf. Therm. Eng. 1851 (1) (2017) 020016, https://doi.org/10.1063/1.4984645.
[48] H. Xu, C.H. Zhang, N. Wang, Z.H. Qu, S.H. Zhang, Experimental study on the performance of a solar photovoltaic/thermal system combined with phase change material, Sol. Energy 198 (2020) 202–211, https://doi.org/10.1016/j.solener.2020.01.064.
[49] D. Korres, C. Tzivanidis, Thermal analysis of a serpentine flat plate collector and investigation of the flow and convection regime, Therm. Sci. 23 (2019) 47–59, https://doi.org/10.2298/TSCI161130172K.
[50] R. Shah, P. Srinivasan, Hybrid photovoltaic and solar thermal systems (PVT): performance simulation and experimental validation, Mater. Today: Proc. 5 (2018) 22998–23006, https://doi.org/10.1016/j.matpr.2018.11.028.
[51] M.M. Sardouei, H. Mortezapour, K. Jafari Naeimi, Temperature distribution and efficiency assessment of different PVT water collector designs, Sādhanā 43 (2018), https://doi.org/10.1007/s12046-018-0826-x.
[52] A.H.A. Al-Waeli, K. Sopian, M.T. Chaichan, H.A. Kazem, A. Ibrahim, S. Mat, Evaluation of the nanofluid and nano-PCM based photovoltaic thermal (PVT) system: an experimental study, Energy Convers. Manag. 151 (2017) 693–708, https://doi.org/10.1016/j.enconman.2017.09.032.
[53] M. Rosli, S. Misha, K. Sopian, S. Mat, M.Y. Sulaiman, E. Salleh, Parametric analysis on heat removal factor for a flat plate solar collector of serpentine tube, World Appl. Sci. J. 29 (2014) 184–187, https://doi.org/10.5829/idosi.wasj.2014.29.02.1357.
[54] A. Kumar, Performance of solar flat plate by using semi-circular cross-sectional tube, Int. J. Eng. Res. Gen. Sci. 2 (2014) 33–37.

[55] P. Razi, M.A. Akhavan-Behabadi, M. Saeedinia, Pressure drop and thermal characteristics of CuO-base oil nanofluid laminar flow in flattened tubes under constant heat flux, ICMHT 38 (2011) 964–971, https://doi.org/10.1016/j.icheatmasstransfer.2011.04.010.

[56] A. Ibrahim, M.Y. Othman, M.H. Ruslan, M. Alghoul, Performance of photovoltaic thermal collector (PVT) with different absorbers design, WSEAS Trans. Environ. Dev. 5 (2009) 321–330.

[57] A. Sohani, C. Cornaro, M.H. Shahverdian, S. Samiezadeh, S. Hoseinzadeh, A.R. Dehghani-Sanij, Using Building Integrated Photovoltaic Thermal (BIPV/T) systems to achieve net zero goal: current trends and future perspectives, in: Towards Net Zero Carbon Emissions in the Building Industry, Springer, New York, 2022, pp. 91–107. https://10.1007/978-3-031-15218-4_5.

[58] A. Nahar, M. Hasanuzzaman, S. Parvin, Computational modeling for photovoltaic thermal system. International Conference on Computing Advancements, 2020, pp. 1–7, https://doi.org/10.1145/3377049.3377129.

[59] H. Fayaz, R. Nasrin, N.A. Rahim, M. Hasanuzzaman, Energy and exergy analysis of the PVT system: effect of nanofluid flow rate, Sol. Energy 169 (2018) 217–230, https://doi.org/10.1016/j.solener.2018.05.004.

[60] J.H. Lee, S.G. Hwang, G.H. Lee, Efficiency improvement of a photovoltaic thermal (PVT) system using nanofluids, Energies 12 (2019) 3063, https://doi.org/10.3390/en12163063.

[61] J.A. Duffie, W.A. Beckman, N. Blair, Solar Engineering of Thermal Processes, Photovoltaics and Wind, John Wiley & Sons, New York, 2020, pp. 244–330, https://doi.org/10.1002/9781119540328.